Extension of ZVS Region of Series–Series WPT Systems by an Auxiliary Variable Inductor for Improving Efficiency

Yong Li, *Member, IEEE*, Shunpan Liu, Xiao Zhu, Jiefeng Hu, *Senior Member, IEEE*, Min Zhang, Ruikun Mai, *Member, IEEE*, and Zhengyou He, *Senior Member, IEEE*

***Abstract*—To maintain a stable output voltage under various operating conditions without introducing extra dc/dc converters, phase-shift (PS) control is usually adopted for wireless power transfer (WPT) systems. By using this method, however, zero-voltage switching (ZVS) operation cannot be guaranteed, especially in light-load conditions. To achieve high efficiency and reduce electromagnetic interference, it is significant for WPT systems to achieve ZVS operation of all switching devices in the whole operation range. In this article, an auxiliary variable inductor, of which the equivalent inductance can be controlled by adjusting the dc current in its auxiliary winding, is designed for series–series-compensated WPT systems under PS control to mitigate the loss arising from hard switching. As a result, a wide ZVS operation range of all switching devices can be achieved. A laboratory prototype is built to verify the theoretical analysis. The experimental results show that, under load and magnetic coupling variations, ZVS operation at fixed operation frequency as well as a constant dc output voltage can be maintained. Compared to the conventional method with only PS control, the proposed WPT can achieve higher overall efficiency in a wider load range owing to the wide ZVS operation range.**

***Index Terms*—Phase-shift (PS) control, variable inductor (VI), wireless power transfer (WPT), zero-voltage switching (ZVS).**

I. Introduction

WIRELESS power transfer (WPT) is an emerging technology that can deliver power from the primary side to the secondary side without physical contact. In the past few years, it has become popular and has been widely applied in various applications, e.g., consumer electronics and electric vehicles, due to its unique merits including safety, convenience, and reliability [1]–[7].

For a typical WPT system, a high-frequency full-bridge inverter as a power supply is usually used to generate a high-frequency current in the primary side. The power loss of the high-frequency inverter accounts for an important portion of the overall power losses of the WPT system. In practice, the power switches used in the high-frequency inverter are usually power MOSFETs, and their ON-resistances are very small. The main power loss of the inverter is therefore the hard-switching loss, which lowers the efficiency of the WPT system. In this sense, it is significant for the high-frequency inverter to achieve the zero-voltage switching (ZVS) in the whole operation range in order to improve overall efficiency and reduce electromagnetic interference (EMI).

In addition to the ZVS operation, a stable output voltage or current ability is another significant concern for WPT systems. In practice, the output voltage of a WPT system is affected by many factors, e.g., load conditions, mutual inductance, etc. Under such circumstance, an advanced WPT system is desired to provide constant and stable output voltage for the load, e.g., batteries, against mutual inductance and load variations [2].

To realize these two objectives, many researchers have made great efforts and proposed numerous control methods [8]–[11]. Such methods can be classified into four categories. The first type is to use a dc–dc converter at the primary side or secondary side to achieve the desired output voltage [12]. The gate driving signals of the inverter switches are kept constant at 50% duty cycle with a fixed switching frequency. In this case, the inverter can easily achieve ZVS operation under resonant condition. However, the additional dc–dc converter brings in drawbacks, such as extra power losses, increased cost, and bulky size.

To avoid using extra dc–dc converters, phase-shift (PS) control is usually adopted for the primary-side high-frequency inverter. By adjusting the conduction angle, a stable output voltage at the secondary side under various operation conditions can be achieved [2]. Unfortunately, this method cannot achieve ZVS operation of the inverter in the whole operation range, especially in light-load condition, leading to high switching power losses and low efficiency [13], [14].

Manuscript received May 28, 2020; revised September 24, 2020; accepted November 17, 2020. Date of publication December 2, 2020; date of current version March 5, 2021. This work was supported in part by the Chengdu Guojia Electrical Engineering Company, Ltd., under Grant NEEC-2018-B05, in part by the National Natural Science Foundation of China under Grant 51907169, in part by the Sichuan Science and Technology Program under Grant 2020YFH0031, and in part by the Fundamental Research Funds for the Central Universities under Grant 2682020CX16. Recommended for publication by Associate Editor D. Dujic. *(Corresponding author: Zhengyou He.)*

Yong Li is with the National Rail Transit Electrification and Automation Engineering Technique Research Center and the School of Electrical Engineering, Southwest Jiaotong University, Chengdu 610031, China (e-mail: leeo1864@163.com).

Shunpan Liu, Xiao Zhu, Min Zhang, Ruikun Mai, and Zhengyou He are with the School of Electrical Engineering, Southwest Jiaotong University, Chengdu 610031, China (e-mail: liusp@my.swjtu.edu.cn; zhuxiaoswjtu@163.com; xnjdzm@qq.com; 82009003@qq.com; hezy@home.swjtu.edu.cn).

Jiefeng Hu is with the School of Engineering, Information Technology and Physical Sciences, Federation University Australia, Mount Helen, VIC 3353, Australia (e-mail: j.hu@federation.edu.au).

Color versions of one or more figures in this article are available at https://doi.org/10.1109/TPEL.2020.3042011.

Digital Object Identifier 10.1109/TPEL.2020.3042011

Another possible method for achieving ZVS operation without using dc–dc converters is to adjust the operation frequency of the WPT system [15]–[17]. The selected operation frequency should be higher than the resonant frequency to guarantee the ZVS operation. Nevertheless, there may be multiple frequencies that can achieve ZVS operation. This is widely recognized as the bifurcation phenomenon, leading to systematic instability [18], [19]. Therefore, to avoid the bifurcation phenomena, fixed operation frequency is preferred.

Meanwhile, a combination of PS control and variable frequency control strategy is proposed to control the inverter of the WPT system flexibly [16]. The PS control is used to regulate the output voltage, and the variable frequency control is used to adjust the impedance angle to achieve ZVS operation [17]–[20]. Besides, an enhanced phase detection methodology is proposed to measure the phase of resonant current. But once again, by using variable frequency control, the resonant condition of the secondary side will be changed, which will affect the overall efficiency [21]. It has been pointed out that the WPT system can achieve a high efficiency when the operating frequency is the resonant frequency of the secondary side [21].

In fact, the essences of achieving ZVS operations are to regulate the equivalent impedance of reactive components [18]. Thus, the input impedance of the WPT system should be adjusted dynamically with respect to the load or mutual inductance, thereby providing the possibility for achieving ZVS operations. Actually, apart from changing the operation frequency, variable inductors (VIs) have been widely used in power electronics applications such as LEDs and electronic ballasts to regulate the equivalent impedance in the resonant circuit [22], [23]. The equivalent inductance of the VI can be continuously altered by the dc current in its auxiliary winding [22]–[24]. Meanwhile, the VI has been used to dynamically match the secondary resonant circuit of the WPT system to achieve a stable resonant frequency [24].

In light of these, the VI finds its new application in WPT systems to extend the ZVS operation range. In this article, a simple and effective method is proposed to extend the ZVS operation range based on an auxiliary VI installed in the primary side. The PS control method is also used for the WPT system with fixed operation frequency to achieve a stable output voltage against mutual inductance and load variations.

The main contributions of this article are listed as follows.

1) A novel control method, the coordination of PS control and a VI at the primary side, is proposed to extend the ZVS region of the series–series (SS)-compensated WPT systems. By dynamically regulating the conduction angle of the inverter, the system dc output voltage can be maintained at a constant level against varying mutual inductances and loads. Meanwhile, with an extra impedance angle altered by the VI, the ZVS operation of the inverter can be achieved with a fixed operation frequency. As a result, compared with the conventional PS control, the conduction angle of the inverter can be larger, which further extends the ZVS operation range and improves the system overall efficiency.

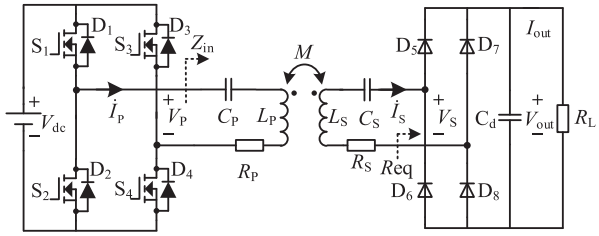

Fig. 1. Circuit diagram of the conventional WPT system.

2) Considering the implementation of constant dc output voltage and ZVS operation, the design procedure of the VI is elaborated. The reactive power in the primary side, equivalent drain–source capacitance of the power MOSFETs, and the performance of the gate driver circuit are all taken into account. Based on these, not only can the ZVS operation be actually realized, but also the reactive power can be minimized.
3) The control diagram of the cooperation of the PS control and the VI is proposed, which consists of two closed control loops. The experimental results show that, with these control loops, desired constant dc output voltage and ZVS operation are simultaneously realized with mutual inductance and load variations, and the system overall efficiency is apparently improved.

II. Analysis of the SS-Compensated WPT System With Conventional PS Control

The SS-compensated WPT system with conventional PS control method is depicted in Fig. 1. $V_{\rm dc}$ and $I_{\rm dc}$ are the dc input voltage and current at the primary side. $V_{\rm out}$ and $I_{\rm out}$ are the dc output voltage and current at the secondary side. The mutual inductance between the primary and the secondary sides is denoted as M. $L_{\rm p}$ and $L_{\rm s}$ are self-inductances of the primary and secondary coil of the magnetic coupler, respectively. Meanwhile, $C_{\rm P}$ and $C_{\rm S}$ denote the series-resonant capacitors. $R_{\rm P}$ is the equivalent series resistance (ESR) of the resonant elements at the primary side (including the primary coil $L_{\rm P}$ and the resonant capacitor $C_{\rm P}$), and $R_{\rm S}$ is the total ESR of the secondary coil and the resonant capacitor $C_{\rm S}$. To compensate the self-inductance of coils at both primary and secondary side, $C_{\rm P}$ and $C_{\rm S}$ should satisfy the following requirement:

$$\omega = \frac{1}{\sqrt{L_{\rm P}C_{\rm P}}} = \frac{1}{\sqrt{L_{\rm S}C_{\rm S}}} \tag{1}$$

where $\omega = 2\pi f$ is the system operating angular frequency; f is the system operating frequency.

The inverter is controlled by the PS modulation, and the key operation waveforms of the WPT system are shown in Fig. 2. The gates' driving signals ($v_{\rm GS\cdot S1}$−$v_{\rm GS\cdot S4}$) with 50% duty cycle at the same leg are complementary to each other at the operation angular frequency ω. A dead time $\delta_{\rm d}$ is set to prevent short circuit at the same leg. Besides, a phase difference between $v_{\rm GS\cdot S1}$ and $v_{\rm GS\cdot S4}$ (and between $v_{\rm GS\cdot S2}$ and $v_{\rm GS\cdot S3}$) is introduced to generate a quasi-square voltage $v_{\rm p}$ with conduction angle α.

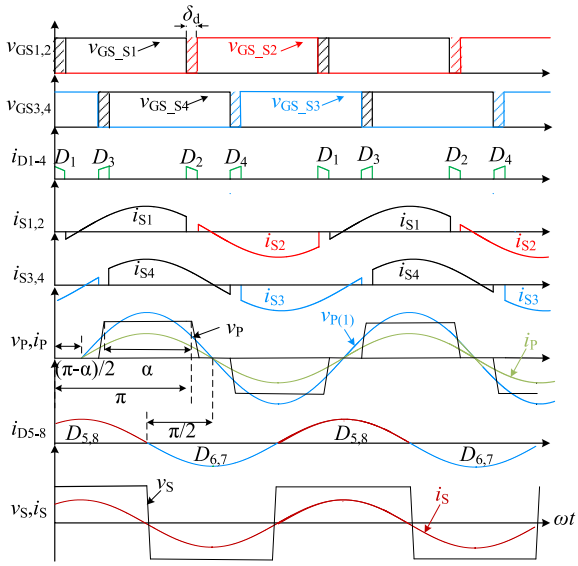

Fig. 2. Operation waveforms of the inverter with conventional control method.

$v_{p(1)}$ is the fundamental component of v_p. i_p and i_s are currents in the primary coil and the secondary coil, respectively. R_{eq} is the equivalent resistance of the rectifier, i.e.,

$$R_{eq} = \frac{8}{\pi^2} R_L. \tag{2}$$

According to Fourier decomposition, the voltage v_P in time domain can be expressed as

$$v_P = \frac{4}{\pi} V_{dc} \sin\frac{\alpha}{2} \sum_{n=1,3,5\cdots}^{+\infty} \frac{\sin\left(n\omega t - \frac{\pi-\alpha}{2}\right)}{n}. \tag{3}$$

The fundamental harmonic approximation (FHA) method is used to analyze the WPT system since the resonant fundamental current is considerably larger than harmonics due to the resonant network [1], [2]. According to the fundamental harmonic analysis, the fundamental voltage of the inverter can be derived as

$$v_{P(1)} = \frac{4}{\pi} V_{dc} \sin\frac{\alpha}{2} \sin\left(\omega t - \frac{\pi-\alpha}{2}\right). \tag{4}$$

The root-mean-square (rms) value of the inverter fundamental output voltage and the rectifier fundamental input voltage can be expressed as

$$V_{P(1)} = \frac{2\sqrt{2}}{\pi} V_{dc} \sin\frac{\alpha}{2} \tag{5}$$

$$V_S = \frac{2\sqrt{2}}{\pi} V_{out} \tag{6}$$

where α is the conducting angle of the inverter, as shown in Fig. 2. By regulating α, the fundamental component of V_p can be adjusted to suit the output voltage requirement with varying load and mutual inductance. Meanwhile, denoting the rms value of the primary current and the secondary current as I_P and I_S, the dc input current I_{dc} and the dc output current I_{out} can be expressed as

$$I_{dc} = \frac{2\sqrt{2}}{\pi} I_P \sin\frac{\alpha}{2} \tag{7}$$

$$I_{out} = \frac{2\sqrt{2}}{\pi} I_S. \tag{8}$$

According to Kirchhoff's voltage law and the mutual coupling theory, the following equation can be obtained:

$$\begin{cases} \dot{V}_{P(1)} = [-jX_{CP} + jX_{LP} + R_P]\,\dot{I}_P + jX_M\dot{I}_S \\ 0 = jX_M\dot{I}_P + (jX_{LS} - jX_{CS} + R_{eq} + R_S)\,\dot{I}_S \end{cases} \tag{9}$$

where

$$\begin{cases} X_{LP} = \omega L_P \; X_{CP} = 1/\omega C_P \\ X_M = \omega M \; X_{LS} = \omega L_S \; X_{CS} = 1/\omega C_S. \end{cases} \tag{10}$$

The currents in the primary coil and the secondary coil can be solved by combining (1), (9), and (10) as

$$\dot{I}_P = \frac{\dot{V}_{P(1)} \cdot (R_{eq} + R_S)}{\omega^2 M^2 + R_P\,(R_{eq} + R_S)} \tag{11}$$

$$\dot{I}_S = -\frac{j\omega M \dot{V}_{P(1)}}{\omega^2 M^2 + R_P\,(R_{eq} + R_S)}. \tag{12}$$

The output voltage V_{out} can be obtained by combining (2), (8), and (12) as

$$V_{out} = I_{out} \cdot R_L = \frac{\omega M V_{dc} \sin\frac{\alpha}{2} R_{eq}}{R_P\,(R_S + R_{eq}) + \omega^2 M^2}. \tag{13}$$

Apparently, according to (13), to maintain the dc output voltage V_{out} at a constant value with various load resistance R_L, α should be regulated by

$$\alpha = 2\arcsin\left\{\frac{V_{out}\left[R_P\,(R_S + R_{eq}) + \omega^2 M^2\right]}{V_{dc}\omega M R_{eq}}\right\}. \tag{14}$$

Meanwhile, according to (11), the equivalent impedance of the inverter Z_{in} can be deduced as

$$Z_{in} = \frac{\dot{V}_{P(1)}}{\dot{I}_P} = R_P + \frac{\omega^2 M^2}{R_{eq} + R_S}. \tag{15}$$

When both the primary side and the secondary side are completely resonant, according to (15), it is obvious that the input impedance angle β of the WPT system (the zero-crossing phase of i_P) is zero, since the equivalent impedance Z_{in} only has real part. Then, when the input dc voltage *V*dc is fixed, according to (13), to achieve a constant output voltage V_{out}, α should be decreased when the output power decreases (the load R_L increases). On the other hand, as shown in Fig. 2, the fundamental component of the output voltage of the inverter $v_{p(1)}$ and the current in the primary coil i_P are in phase, which causes the failure of ZVS operation. Thus, switching loss increases when the inverter is controlled by the PS method [25].

In order to clarify the main factors affecting the energy transmission efficiency of the system, the establishment of a loss analysis model is essential. Power losses of WPT systems can generally be divided into two parts. One is the power loss in the passive elements, and the other is the converters loss [25], [26].

The system efficiency of the SS-compensated WPT system can be derived as

$$\eta = \frac{P_{\rm out}}{P_{\rm in}} = \frac{P_{\rm out}}{P_{\rm out} + P_{\rm ESR\_loss} + P_{\rm inverterter\_loss} + P_{\rm rectifier\_loss}} \tag{16}$$

where $P_{\rm out}$ and $P_{\rm in}$ are dc input power and output power, respectively; $P_{\rm inverter\_loss}$ is the power loss of the inverter (including the conducting loss and the switching loss); $P_{\rm rectifier\_loss}$ is the power loss of the passive rectifier; $P_{\rm ESR\_loss}$ is the power loss of the passive elements.

Apparently, the power loss of each part is related to the current in the primary coil or the secondary coil. According to Fig. 2, to describe the real-time values of the currents, $i_{\rm p}$ and $i_{\rm S}$ can be defined as

$$i_{\rm P} = \sqrt{2} I_{\rm P} \sin\left(\omega t - \frac{\pi - \alpha}{2}\right) \tag{17}$$

$$i_{\rm S} = \sqrt{2} I_{\rm S} \sin\left(\omega t + \frac{\alpha}{2}\right). \tag{18}$$

Meanwhile, to describe the switching process for analyzing the power loss of each part, the waveforms of the current flows in the coils, MOSFETs, and its antiparallel diodes are illustrated in Fig. 2.

To analyze the power loss in each part of the system with the conventional PS control, especially the switching loss of the inverter, a calculation model of the power loss should be well established. Here, the system power loss can be divided into the following parts.

1) Power Losses of the Passive Elements: The power losses in the passive elements can be divided into the power loss in the primary side and that in the secondary side, which are determined by the ESRs and the rms values of the currents. The total power loss in the passive elements can be expressed as

$$P_{\rm ESR\_loss} = R_{\rm P} {I_{\rm P}}^2 + R_{\rm S} {I_{\rm S}}^2. \tag{19}$$

2) Power Losses of the Inverter: The power loss of the inverter consists of conduction loss and switching loss of the MOSFETs and its antiparallel diodes [25], [26]. Each part of the losses can be calculated based on the inherent parameters of the inverter.

First, as shown in Fig. 2, the conducting loss of the MOSFETs is determined by the output current of the inverter $i_{\rm p}$, the condition time, and the drain–source ON-state resistance $r_{\rm m}$, which can be calculated by

$$P_{\rm mos} = \frac{2}{\pi} I_{\rm P}^2 r_{\rm m} \left[\pi - \delta_{\rm d} + \frac{1}{2}\left(\sin\alpha - \sin\left(\alpha + 2\delta_{\rm d}\right)\right)\right]. \tag{20}$$

Second, the conducting loss of the diodes is produced during the period of $\delta_{\rm d}$, when the MOSFETs are switching. Thus, the conducting loss of the diodes can be expressed as

$$P_{\rm diode} = \frac{2\sqrt{2}}{\pi} V_{\rm if} I_{\rm P} \left(\sin\left(\frac{\alpha}{2} + \delta_{\rm d}\right) - \sin\frac{\alpha}{2}\right) + \frac{2}{\pi} r_{\rm id} I_{\rm P}^2 \left[\delta_{\rm d} + \frac{1}{2}\left(\sin\left(\alpha + 2\delta_{\rm d}\right) - \sin\alpha\right)\right] \tag{21}$$

where $V_{\rm if}$ is the diode forward voltage; $r_{\rm id}$ is the equivalent ON-state resistance of the antiparallel diodes. Due to the short dead time $\delta_{\rm d}$, this part of the power loss only accounts for a small percentage of the overall power loss [25], [26].

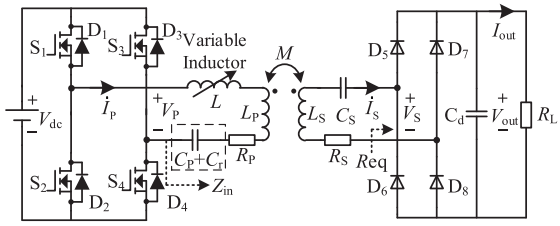

Fig. 3. Circuit diagram of the proposed WPT system with a primary-side VI.

Third, as seen from Fig. 2, there are four switching states within each switching period. When the inverter is operating without the ZVS condition, the switching power loss of the inverter, including the switching loss of the MOSFETs and their antiparallel diodes, can be calculated as [25], [26]

$$P_{\rm sw} = 2\sqrt{2} V_{\rm dc} I_{\rm P} \left|\cos\left(\frac{\alpha}{2}\right)\right| \left(\frac{E_{\rm on} + E_{\rm off}}{V_{\rm DD} I_{\rm D}} + \frac{Q_{\rm DD}}{I_{\rm R\_D}}\right) f \tag{22}$$

where $E_{\rm on}$ and $E_{\rm off}$ are, respectively, the turn-ON and turn-OFF energy losses of MOSFET; $V_{\rm DD}$ and $I_{\rm D}$ are respectively, the reference drain–source voltage and source current of MOSFET; and $Q_{\rm DD}$ and $I_{\rm R\_D}$ are the reverse recovery charge and the reference current of the diode, respectively. For the WPT system, the switching loss always occupies a large part of the overall power loss, due to the limitation of the switching performance of the MOSFETs [25], [26].

Therefore, the total power loss of the inverter can be calculated as

$$P_{\rm inverter\_loss} = P_{\rm mos} + P_{\rm diode} + P_{\rm SW}. \tag{23}$$

3) Power Losses of the Rectifier: For the passive rectifier at the secondary side, the power loss is mainly the conduction loss of the diodes, which can be derived as

$$P_{\rm rectifier\_loss} = \frac{4\sqrt{2}}{\pi} V_{\rm rf} I_{\rm S} + 2 r_{\rm rd} I_{\rm S}^2 \tag{24}$$

where $V_{\rm rf}$ is the diode forward voltage and $r_{\rm rd}$ is the equivalent ON-state resistance of the diodes in the rectifier.

III. Analysis of the SS-Compensated WPT System With the Proposed Control Method

A. Operation Analysis of PS Control With a VI

As shown in Fig. 3, the proposed WPT method contains an extra VI that is series-connected at primary side, and its series-connected capacitance $C_{\rm r}$ can be combined with resonant capacitors $C_{\rm P}$ into a new one. The structure and its implementation are shown in Fig. 4. The VI consists of two windings, i.e., the main winding and the auxiliary winding [20]–[24]. The main winding is wounded in the middle leg of the EE-shape ferrite core that contains an air gap, and the auxiliary winding is placed in the lateral legs, as shown in Fig. 4(a). $N_{\rm b}$ and $N_{\rm p}$ are the turns of the auxiliary and the main windings, respectively. In order to cancel the induced ac voltage in the auxiliary winding,

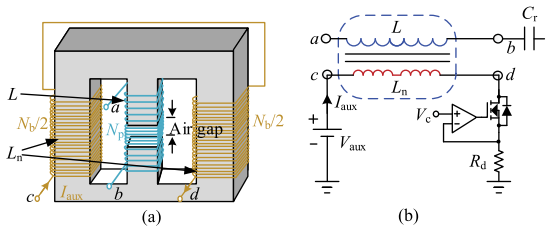

Fig. 4. (a) Structure of the VI. (b) Implementation of the VI using a linear current source.

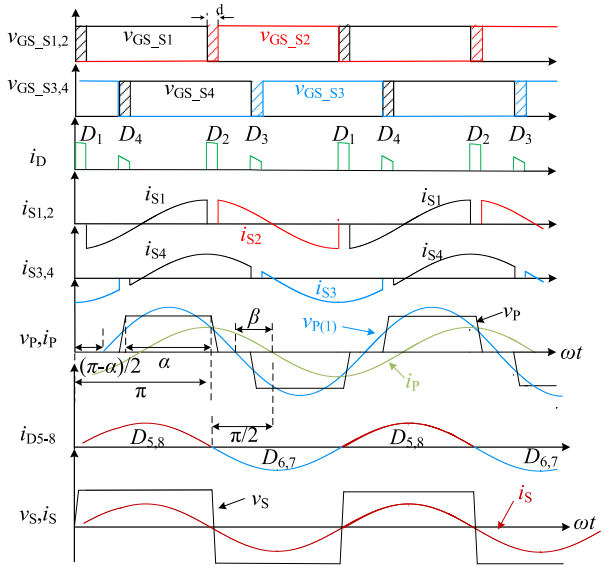

Fig. 5 Operation waveforms of the inverter with the proposed control method.

the winding in the lateral legs should be serially connected in opposite polarity.

According to [20]–[24], the inductance of the main winding can be continuously adjusted by altering the dc current through the auxiliary winding. In this article, a simple linear circuit is used to implement the controllable dc current [20]–[24], as shown in Fig. 4(b). The linear circuit is supplied by an auxiliary dc voltage $V_{\rm aux}$. By controlling the reference voltage $V_{\rm c}$, a desired dc current $I_{\rm aux}$ can be achieved [20]–[24].

Similarly, the key operation waveforms of the proposed WPT system are shown in Fig. 5. The inverter is regulated by the PS control method, while the VI can affect the input impedance angle β. The KVL equations can be established as

$$\begin{cases} \dot{V}_{\rm P(1)} = \left[-jX_{\rm CP} + jX_{\rm LP} + jX_{\rm L} + R_{\rm P}\right]\dot{I}_{\rm P} + jX_{\rm M}\dot{I}_{\rm S} \\ 0 = jX_{\rm M}\dot{I}_{\rm P} + \left(jX_{\rm LS} - jX_{\rm CS} + R_{\rm eq} + R_{\rm S}\right)\dot{I}_{\rm S}. \end{cases} \tag{25}$$

Substituting (10) to (25), the currents in both the primary coil and the secondary coil can be solved as

$$\dot{I}_{\rm P} = \frac{\dot{V}_{\rm P(1)} \cdot (R_{\rm eq} + R_{\rm S})}{\omega^2 M^2 + R_{\rm P}(R_{\rm eq} + R_{\rm S}) + j\omega L(R_{\rm eq} + R_{\rm S})} \tag{26}$$

$$\dot{I}_{\rm S} = -\frac{j\omega M \dot{V}_{\rm P(1)}}{\omega^2 M^2 + R_{\rm P}(R_{\rm eq} + R_{\rm S}) + j\omega L(R_{\rm eq} + R_{\rm S})}. \tag{27}$$

Moreover, combining (2), (8), and (27), the dc output voltage $V_{\rm out}$ can be obtained as

$$V_{\rm out} = \frac{\omega M V_{\rm dc} \sin\frac{\alpha}{2} R_{\rm eq}}{\sqrt{\left[\omega L(R_{\rm S} + R_{\rm eq})\right]^2 + \left[R_{\rm P}(R_{\rm S} + R_{\rm eq}) + \omega^2 M^2\right]^2}}. \tag{28}$$

Meanwhile, according to (26), the equivalent impedance of the inverter $Z_{\rm in}$ can be also deduced as

$$Z_{\rm in} = \frac{\dot{V}_{\rm P(1)}}{\dot{I}_{\rm P}} = R_{\rm P} + \frac{\omega^2 M^2}{R_{\rm eq} + R_{\rm S}} + j\omega L. \tag{29}$$

According to (28), to provide a constant dc output voltage $V_{\rm out}$, the conduction angle α should satisfy

$$\alpha = 2\arcsin \times \left\{ \frac{V_{\rm out}\sqrt{\left[\omega L(R_{\rm S} + R_{\rm eq})\right]^2 + \left[R_{\rm P}(R_{\rm S}+R_{\rm eq}) + \omega^2 M^2\right]^2}}{V_{\rm dc}\omega M R_{\rm eq}} \right\}. \tag{30}$$

Similarly, considering (29), the input impedance angle β can be obtained as

$$\beta = \arctan\left(\frac{\omega L(R_{\rm eq} + R_{\rm S})}{R_{\rm P}(R_{\rm eq} + R_{\rm S}) + \omega^2 M^2}\right). \tag{31}$$

According to (31), it is obvious that there is an extra phase difference β between $v_{\rm p}$ and $i_{\rm p}$ due to the extra impedance of the VI. Thus, the ZVS operation can be actually achieved by adjusting the equivalent impedance of the VI. Besides, according to (30), when the system load resistance and output power are fixed, with a phase difference β between $v_{\rm p}$ and $i_{\rm p}$, α can be smaller compared to the WPT system without VI. As a result, the ZVS condition can be fulfilled over a wide load range [15], [16]. When the ZVS operation is actually achieved, the system efficiency of the proposed WPT system is expressed as

$$\eta = \frac{P_{\rm out}}{P_{\rm in}} = \frac{P_{\rm out}}{P_{\rm out} + P_{\rm ESR\_loss} + P_{\rm inverter\_loss} + P_{\rm rectifier\_loss} + P_{\rm VI\_DC}} \tag{32}$$

where $P_{\rm VI\_DC}$ is the power loss in the linear circuit of the VI.

In order to calculate the power loss of each part, describing the real-time values of the currents in the primary coil and the secondary coil are still necessary. However, in the proposed WPT system, the phase of $i_{\rm P}$ will be delayed by β compared to the phase of $v_{\rm P}$. Therefore, $i_{\rm P}$ and $i_{\rm S}$ can be defined as

$$i_{\rm P} = \sqrt{2} I_{\rm P} \sin\left(\omega t - \frac{\pi - \alpha}{2} - \beta\right) \tag{33}$$

$$i_{\rm S} = \sqrt{2} I_{\rm S} \sin\left(\omega t + \frac{\alpha}{2} - \beta\right). \tag{34}$$

Similarly, to theoretically calculate and judge the efficiency improvement caused by achieving the ZVS operation with the VI, a calculation model of the power loss is also necessary. The mathematical model of the system power loss can be established as follows.

1) Power Losses of the Passive Elements

In the proposed WPT system, the passive elements at the primary side include not only the primary coil L_{P} and the series-resonant capacitor C_{P}, but also the VI. Thus, the total power loss in the passive elements can be expressed as

$$P_{\mathrm{ESR\_loss}} = (R_{\mathrm{P}} + R_{\mathrm{VI}})\, {I_{\mathrm{P}}}^2 + R_S {I_{\mathrm{S}}}^2 \tag{35}$$

where R_{VI} is the ESR of the VI in the ac side.

2) Power Losses of the Inverter

Due to the input impedance angle β caused by the VI, the power loss calculation method of the inverter is also different from that in the conventional SS-compensated WPT system.

First, in the proposed WPT system, the switch moments are shifted by phase difference angle β. Thus, according to the current waveforms in Fig. 5, the conducting loss of the MOSFETs should be calculated by [25], [26]

$$\begin{aligned} &P_{\mathrm{mos}} \\ &= \frac{1}{\pi} r_{\mathrm{m}} I_{\mathrm{P}}^2 \left[\pi - \delta_{\mathrm{d}} + \frac{1}{2}\left(\sin(\alpha + 2\beta - 2\delta_{\mathrm{d}}) - \sin(\alpha + 2\beta)\right)\right] \\ &+ \frac{1}{\pi} r_{\mathrm{m}} I_{\mathrm{P}}^2 \left[\pi - \delta_{\mathrm{d}} + \frac{1}{2}\left(\sin(\alpha - 2\beta) + \sin(2\beta - 2\delta_{\mathrm{d}} - \alpha)\right)\right] \end{aligned} \tag{36}$$

where $P_{\mathrm{S1,2}}$ is the conducting loss of S_1 and S_2, and $P_{\mathrm{S3,4}}$ is the conducting loss of S_3 and S_4.

Second, when the MOSFETs are switching, i_{P} will also flow in the antiparallel diodes of the MOSFETs for a short period δ_{d}. Thus, according to the current waveforms of the diodes in Fig. 5, the conducting loss of the diodes should be expressed as

$$\begin{aligned} &P_{\mathrm{diode}} \\ &= \frac{\sqrt{2}}{\pi} V_{\mathrm{if}} I_{\mathrm{P}} \left[\sin\left(\delta_{\mathrm{d}} - \frac{\alpha}{2} - \beta\right) + \sin\left(\frac{\alpha}{2} + \beta\right)\right] \\ &+ \frac{\sqrt{2}}{\pi} V_{\mathrm{if}} I_{\mathrm{P}} \left[\sin\left(\delta_{\mathrm{d}} + \frac{\alpha}{2} - \beta\right) + \sin\left(\beta - \frac{\alpha}{2}\right)\right] \\ &+ \frac{1}{\pi} r_{\mathrm{id}} I_{\mathrm{P}}^2 \left[\delta_{\mathrm{d}} + \frac{1}{2}\left(\sin(2\delta_{\mathrm{d}} - \alpha - 2\beta) + \sin(\alpha + 2\beta)\right)\right] \\ &+ \frac{1}{\pi} r_{\mathrm{id}} I_{\mathrm{P}}^2 \left[\delta_{\mathrm{d}} + \frac{1}{2}\left(\sin(2\delta_{\mathrm{d}} + \alpha - 2\beta) + \sin(2\beta - \alpha)\right)\right] \end{aligned} \tag{37}$$

where $P_{\mathrm{D1,2}}$ is the conducting loss of D_1 and D_2, and $P_{\mathrm{D3,4}}$ is the conducting loss of D_3 and D_4.

Third, when the ZVS operation is actually achieved, the turn-ON loss of the four MOSFETs can be considered as zero. Only the turn-OFF loss of the MOSFETs and the switching loss of the antiparallel diodes should be taken into account [25], [26]. Therefore, the switching loss of the inverter can be expressed as

$$\begin{aligned} P_{\mathrm{SW}} = 2\sqrt{2} V_{\mathrm{dc}} I_{\mathrm{P}} &\left[\left|\cos\left(\frac{\alpha}{2} - \beta\right)\right| + \left|\cos\left(\frac{\alpha}{2} + \beta\right)\right|\right] \\ &\times \left(\frac{E_{\mathrm{off}}}{V_{\mathrm{DD}} I_{\mathrm{D}}} + \frac{Q_{\mathrm{DD}}}{I_{\mathrm{R\_D}}}\right) f. \end{aligned} \tag{38}$$

TABLE I
SYSTEM SPECIFICATION AND PARAMETER VALUES

Symbol	Parameter	Value	Unit
V_{dc}	System input DC voltage	100	V
V_{out}	System output DC voltage	72	V
L_{P}	Coil inductance of the transmitter	186.27	μH
L_{S}	Coil inductance of the receiver	187.17	μH
R_{P}	Coil resistance of the transmitter	0.25	Ω
R_{S}	Coil resistance of the receiver	0.25	Ω
C_{P}	Resonant capacitance of L_1	18.82	nF
C_{S}	Resonant capacitance of L_2	18.73	nF
M	Mutual inductance between the transmitter and receiver	30-40	μH
R_{L}	Load resistance	30-90	Ω
f	System operating frequency	85	kHz
V_{aux}	Auxiliary voltage	1.5	V

It is worth mentioning that, without the turn-ON loss, the switching loss of the inverter will be decreased dramatically, causing the turn-OFF loss of the MOSFET to be particularly small compared with the turn-ON loss [25], [26]. Therefore, the switching loss can be greatly reduced by achieving the ZVS operation.

Finally, the total power loss of inverter can be calculated as

$$P_{\mathrm{inverter\_loss}} = P_{\mathrm{mos}} + P_{\mathrm{diode}} + P_{\mathrm{sw}}. \tag{39}$$

3) Power Losses of the Rectifier

For the passive rectifier, according to the waveforms of v_{S} and i_{S}, the power loss of the rectifier can be calculated by

$$P_{\mathrm{rectifier\_loss}} = \frac{4\sqrt{2}}{\pi} V_{\mathrm{rf}} I_{\mathrm{S}} + 2 r_{\mathrm{rd}} I_{\mathrm{S}}^2. \tag{40}$$

According to (40), although the phases of v_{S} and i_{S} are shifted, the power loss in the rectifier will not be affected when I_{S} has not been changed.

4) Power Losses of the VI

In addition to the power loss of the ESR of the VI, the extra power loss in the auxiliary linear circuit of the VI $P_{\mathrm{VI\_DC}}$ should be considered, which can be simply expressed as

$$P_{\mathrm{VI\_DC}} = V_{\mathrm{aux}} I_{\mathrm{aux}}. \tag{41}$$

B. POWER LOSS COMPARISON BETWEEN THE CONVENTIONAL PS CONTROL AND THE PS CONTROL WITH VI

In order to verify the theoretical overall efficiency of the proposed control method, the power loss of each part when $R_{\mathrm{L}} = 30\ \Omega$ and $R_{\mathrm{L}} = 60\ \Omega$ will be theoretically calculated here. Meanwhile, the key of the system efficiency improvement can be found. Parameters of the SS-compensated WPT system are listed in Table I, and the type of the MOSFETs and diodes are shown in Table II.

TABLE II
SWITCH DEVICES

Switch	Specifications
MOSFET	IPA90R340C3
Diode	DSEI2X61-06C

TABLE III
LOSSES OF SYSTEM

	Conventional method		Proposed method	
	30Ω	60Ω	30Ω	60Ω
$P_{\text{ESR\_loss}}$	4.28W	2.76W	5.38W	3.21W
$P_{\text{inverter\_loss}}$	18.12W	19.74W	3.67W	4.17W
$P_{\text{rectifier\_loss}}$	5.76W	2.88W	5.76W	2.88W
P_{VI}	——	——	2.10W	2.40W
Total loss	28.16W	25.38W	16.91W	12.66W

1) Loss Calculation of the Conventional PS Control

According to (5), (11), and (12), the rms of primary current and secondary current can be obtained by

$$I_{\text{P}} = \frac{\frac{2\sqrt{2}}{\pi} V_{\text{dc}} \sin\frac{\alpha}{2} \cdot (R_{\text{eq}} + R_{\text{S}})}{\omega^2 M^2 + R_{\text{P}} (R_{\text{eq}} + R_{\text{S}})} \tag{42}$$

$$I_{\text{S}} = \frac{\frac{2\sqrt{2}}{\pi} V_{\text{dc}} \omega M \sin\frac{\alpha}{2}}{\omega^2 M^2 + R_{\text{P}} (R_{\text{eq}} + R_{\text{S}})} \tag{43}$$

where α can be calculated by (30) by using the parameters listed in Table I. Therefore, the power loss of each part can be obtained according to Section II. The calculation results are shown in Table III.

2) Loss Calculation of the Proposed PS Control With the VI

According to (5), (26), and (27), the rms of primary and secondary currents can be obtained by

$$I_{\text{P}} = \frac{\frac{2\sqrt{2}}{\pi} V_{\text{dc}} \sin\frac{\alpha}{2} \cdot (R_{\text{eq}} + R_{\text{S}})}{\sqrt{\left[\omega^2 M^2 + R_{\text{P}} (R_{\text{eq}} + R_{\text{S}})\right]^2 + \left[\omega L (R_{\text{eq}} + R_{\text{S}})\right]^2}} \tag{44}$$

$$I_{\text{S}} = \frac{\frac{2\sqrt{2}}{\pi} V_{\text{dc}} \omega M \sin\frac{\alpha}{2}}{\sqrt{\left[\omega^2 M^2 + R_{\text{P}} (R_{\text{eq}} + R_{\text{S}})\right]^2 + \left[\omega L (R_{\text{eq}} + R_{\text{S}})\right]^2}} \tag{45}$$

where α can be calculated according to (30), and the design method of the value of L will be described in Section IV in detail. Hence, when the ZVS operation is actually achieved by adjusting the equivalent impedance of the VI, the power loss distribution can be obtained according to Section III-A. The calculation results are also shown in Table III.

According to Table III, it is obvious that the inverter loss is dramatically decreased by achieving the ZVS operation in the proposed WPT system. Although the extra power loss of the VI, including the power loss of ESR and the power loss in the auxiliary linear circuit of the VI, is brought in the proposed WPT system, the system overall power loss is still apparently improved. According to (16) and (32), the trajectory of the theoretical efficiency with load resistance can be calculated and plotted in Fig. 6, which dedicates that the proposed method can effectively improve the system overall efficiency.

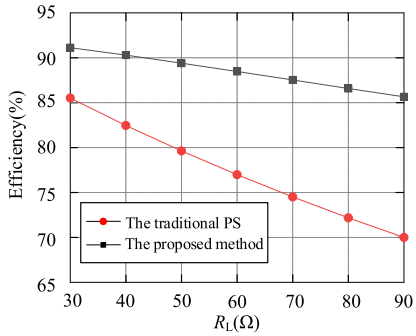

Fig. 6. Efficiency comparison between two methods when $M = 40\,\mu$H.

IV. PARAMETER DESIGN AND CONTROL

By comparing the overall power losses of the conventional PS control and that of the proposed PS control with VI, it is obvious that achieving ZVS operation by adjusting the equivalent impedance of VI can considerably improve the switching loss while the other power losses are not increased apparently. However, for designers, it is important to make the inverter operate in both output voltage regulation and ZVS condition. Thus, to actually realize these design goals, a precise steady-state analysis is necessary.

A. ZVS Condition Analysis and Discussion

According to Fig. 5, in order to achieve the ZVS operation, β must be larger than the phase of $v_{\text{GS\_S4}}$, i.e., [27], [28]

$$\theta \geq 0 \Rightarrow \beta \geq \frac{\pi - \alpha}{2}. \tag{46}$$

For high-frequency inverters, the speed of voltage and current conversion is limited by the switching performance of the gate driver circuit and the equivalent drain–source capacitance of the power MOSFET [29], [30]. Therefore, when the phase difference θ is zero, the ZVS operation will fail. Usually, the phase difference between $v_{\text{GS\_S4}}$ and i_{P}, i.e., θ, is always set as a small positive value for ensuring ZVS operation. On the other hand, with a large θ, it is easy to produce extra reactive power at the primary side, resulting in system efficiency reduction. Thus, to ensure ZVS operation while reducing the reactive power [31], the phase difference θ should track a reference angle δ, which can also simplify the design of the control strategy. The conduction angle α and the input impedance angle β should satisfy

$$\beta = \frac{\pi - \alpha}{2} + \delta. \tag{47}$$

Obviously, to extend the ZVS operation range with the variations of the load R_{L} and to achieve the desired output power, the value of the VI should be carefully designed. Substituting (30) and (31) into (47), the inductance of the VI can be determined

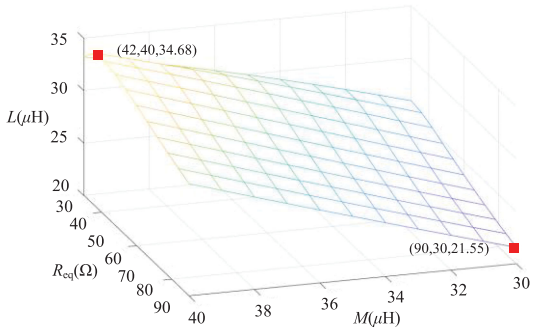

Fig. 7. L as a function of R_{L} and M for the critical ZVS condition.

as

$$L = \frac{\sqrt{\frac{C^2}{2} - B^2 - \frac{A \cdot C}{2}}}{\omega \cdot (R_{\mathrm{eq}} + R_{\mathrm{s}})} \tag{48}$$

where

$$A = C \cdot \cos^2(\delta) - \sin(\delta) \cdot \sqrt{C^2 - (C \cdot \cos(\delta) - 2B)^2} - 2B \cdot \cos(\delta)$$

$$B = R_{\mathrm{p}} \cdot (R_{\mathrm{s}} + R_{\mathrm{eq}}) + \omega^2 M^2$$

$$C = \frac{V_{\mathrm{dc}}}{V_{\mathrm{out}}} \omega \cdot M \cdot R_{\mathrm{eq}}.$$

As can be seen from (48), the exact inductance of the VI for ZVS operation as well as a constant output voltage has been derived. The inductance of the VI must be dynamically adjusted to suit the variations of the load R_{L} and the mutual inductance M. Thus, the structure parameters of the VI should be designed according to the parameters and the power demand of the proposed WPT system.

B. Analysis of the Inductance Range of the VI to Realize the ZVS Operation

In the proposed WPT system, silicon power MOSFETs IPA90R340C3 are chosen in the inverter. In order to ensure the ZVS operation for a wide range, before designing the VI and the control strategy, learning the realization condition of the ZVS operation is necessary. The reference angle needs to be selected according to the actual turn-ON and the turn-OFF times of the MOSFETs that are determined by the inherit characteristics and the gate driver circuit [29], [30]. Here, after careful testing with rated input voltage V_{dc} and different mutual inductances and load resistances, the reference angle δ is set at 15° in this article. With this reference angle δ, ZVS operation can be actually achieved with the wide mutual inductance and load variations listed in Table I.

According to (48), the inductance L versus R_{L} and M are plotted in Fig. 7. It can be found that, with variations of R_{L} and M, L varies on a continuous surface. For example, when the proposed WPT system operates at the condition with $M = 30$ μH and $R_{\mathrm{L}} = 90$ Ω, the minimal inductance of the VI for ZVS is 21.55 μH. When the proposed WPT system operates at the condition with $M = 40$ μH and $R_{\mathrm{L}} = 42$ Ω, the minimal inductance of the VI becomes 34.68 μH to achieve ZVS operation. Therefore, the value of the VI should be from 21.55 to 34.68 μH to ensure ZVS operation, when the load R_{L} is changed from 30 to 90 Ω and M is changed from 30 to 40 μH.

TABLE IV
PARAMETERS OF THE VI

Symbol	Parameter	Value
N_{p}	Turns of the main coil	16
N_{b}	Turns of the auxiliary coil	46
	Air gap	1.0mm
	Total Volume of the VI	70.5mm×66.4mm×32mm

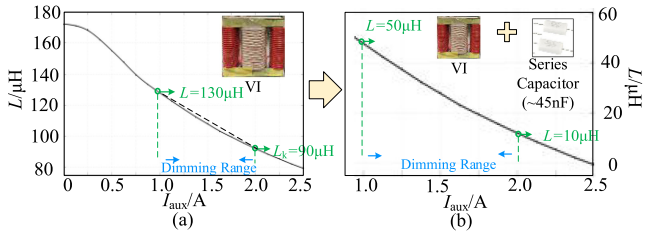

Fig. 8. L against I_{aux} (a) without series capacitor and (b) with series capacitor.

C. Design of the VI

To meet the requirement for ZVS operation specified in Fig. 7, the inductance of the VI should cover the whole range from 21.55 to 34.68 μH. In practice, to ensure the margin of the control system and the operational reliability, the actual range has been designed to be larger than the theoretical range. Meanwhile, to provide a wide cover range of the inductance of the VI, a large number of the main winding turns is necessary.

Besides, as mentioned in [32], the dc current in the auxiliary winding may not be completely stable, due to the fact that there is an unavoidable ac voltage induced by the high-frequency ac current in the main winding. Here, to reduce the induced ac voltage in the auxiliary winding as much as possible, two available methods are adopted. The first one is to connect the auxiliary windings of the lateral legs serially in opposite polarity, while the turns of the two auxiliary windings are set as the same. The other approach is that, the turns of the auxiliary winding N_{b} must be well designed for reducing dc current fluctuation in the auxiliary winding [32]. With the help of LTspice simulation software, the parameters of VI are designed and adjusted, and its optimal turns are finally identified, as shown in Table IV.

Based on the simulation results, the measured relationship between the dc current and the main winding inductance is illustrated in Fig. 8(a). As can be seen, the main winding inductance is inversely proportional to the dc current through the auxiliary winding and hence, it is possible to increase or decrease the control current to change the inductance accordingly. Consequently, the inductance of the main winding ranges from 80 to 172 μH when the dc current changes from 0 to 2 A. It is important to emphasize that, in order to facilitate the design of the controller, the diming range of the VI is preferably limited

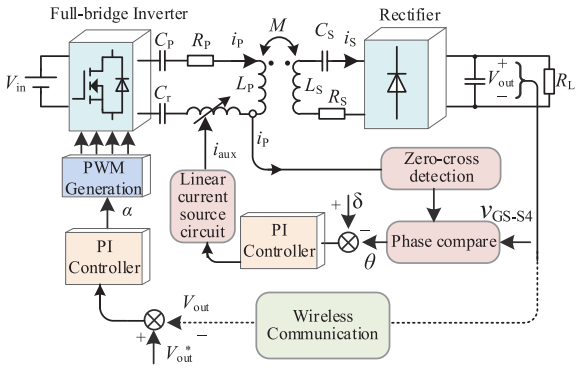

Fig. 9. Proposed control diagram of the WPT system.

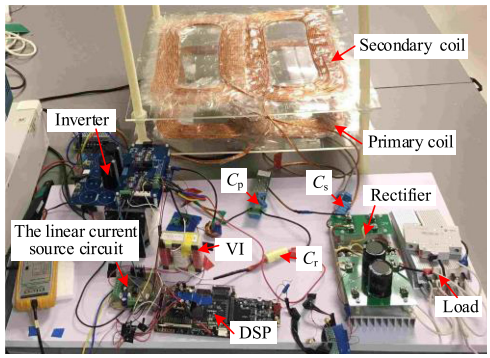

Fig. 10. Experimental prototype.

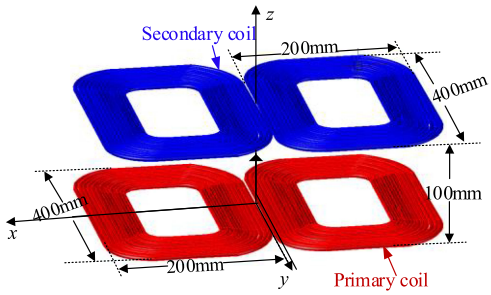

Fig. 11. Model and dimensions of DD coils.

from 90 to 130 μH [see Fig. 8(a)]. In this interval, the variation trend of the VI can be approximately regarded as a linear curve.

To meet the requirement for ZVS operation in the designed system, it is necessary to add an extra series-connected capacitor to compensate the excess part of the inductance. In order to make the dimming range margin, a ~45 nF capacitor is selected. Thus, the diming range of the VI is shifted from 10 to 50 μH, as shown in Fig. 8(b). With this dimming range, the proposed system will operate stably and reliably.

D. Control Diagram

The control diagram is depicted in Fig. 9. It consists of two closed control loops, i.e., the dc output voltage control loop and the ZVS control loop. First, the dc output voltage $V_{\rm out}$ is measured and sent to the primary side for a PI controller through radio frequency (RF) communication. The output of the PI controller is the conduction angle α for controlling the inverter. Second, the ZVS control loop is responsible for ZVS operation of the WPT system. Theoretically, θ should track the reference angle $\delta = 15°$, as explained in Section IV-B.

To implement this, the phase of $i_{\rm P}$ can be obtained by using zero-cross detection. Then, the phase difference between $v_{\rm gs4}$ and $i_{\rm P}$, i.e., θ, can be obtained by the phase comparison circuit. Afterward, the phase difference θ is controlled to track a reference angle δ through a PI controller, by altering the dc current through the auxiliary winding of the VI. By using this two-loop control strategy, the WPT system can achieve a constant output current as well as a wide ZVS operation range.

V. Experimental Results

A. Experimental Prototype

The experimental prototype is shown in Fig. 10 using the parameters in Table. I. A digital signal processor (TMS320F28335) is used as the controller for pulsewidth modulation (PWM) generation with two-loop control strategy. MOSFETs (IPA90R340C3) are used as the switches S_1–S_4.

In this article, the key challenge of the WPT system under consideration is to provide a constant output voltage with ZVS operation subject to various mutual inductances and load resistances. In fact, no matter which direction the secondary coil is misaligned in, the mutual inductance will be affected. Thus, WPT systems should be endowed with tolerance of misalignment and distance variations between the primary coil and the secondary coil. In practical applications, the WPT system is usually designed to have a high tolerance to the lateral misalignment, while the requirements of the misalignment tolerances in the longitudinal and vertical directions are not relatively strict [3], [6], [12], [31].

In this experimental prototype, a pair of Double-D (DD) coils are employed here for both the primary coil and the secondary coil. The finite-element analysis (FEA) software ANSYS MAXWELL is used to design the parameters of the magnetic coupler. The model and the dimensions of the magnetic coupler are shown in Fig. 11. In this prototype, coils are made of 800-strand litz-wire with a diameter of 4.5 mm. The primary and secondary coils are both set as 14 turns.

The simulated and experimental mutual inductances versus x-axis, y-axis, and z-axis misalignment are shown in Fig. 12. It can be seen that the mutual inductance can be maintain in the range from ~30 to ~40 μH when $x \in [0\,\text{mm}, 50\,\text{mm}]$, $y \in [0\,\text{mm}, 110\,\text{mm}]$, $z \in [85\,\text{mm}, 105\,\text{mm}]$, which are set as the movement range of the secondary coil.

B. ZVS Operation Analysis

The reference voltage $V_{\rm c}$ should be regulated according to the zero-cross detection and phase comparison to achieve variable inductance. Therefore, the ZVS operation can be realized when the VI is dynamically adjusted. The key waveforms of the switch S_4 are analyzed to verify the ZVS operation of proposed WPT

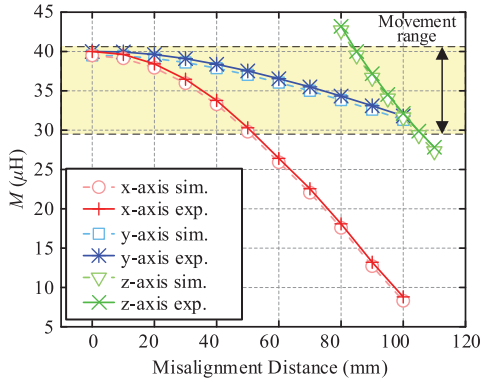

Fig. 12. Variation of mutual inductances due to misalignment of secondary coil.

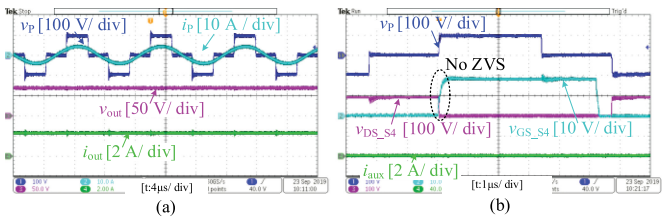

Fig. 13. Experimental waveforms of the WPT system without a VI when $R_{\mathrm{L}} = 30\,\Omega$. (a) Waveforms of v_{P}, i_{P}, v_{out}, i_{out}, and (b) waveforms of S_4.

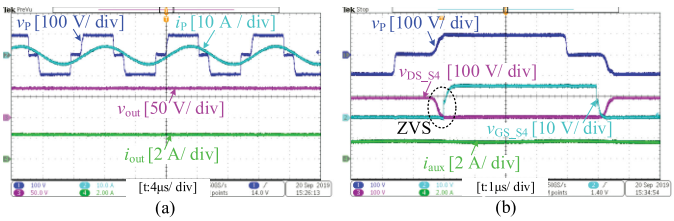

Fig. 14. Experimental waveforms of the WPT system with a VI when $R_{\mathrm{L}} = 30\,\Omega$. (a) Waveforms of v_{P}, i_{P}, v_{out}, i_{out}, and (b) waveforms of S_4.

system since the switches in the lagging leg are more difficult for realizing ZVS operation [31].

Fig. 13(a) shows the experimental results of the inverter's output voltage/current and the dc output current/voltage when the WPT system only uses the PS control under the condition of $M = 40\ \mu$H and $R_{\mathrm{L}} = 30\ \Omega$. The dc output voltage can be controlled as 72 V when the input dc voltage is 100 V. In this case, it can be clearly seen in Fig. 13(b) that the ZVS operation cannot be achieved, which results in high switching power losses. Consequently, the measured overall efficiency (dc–dc efficiency) is only about 86%.

Fig. 14 shows the corresponding waveforms of the WPT system by using the proposed method under the same condition, i.e., $M = 40\ \mu$H and $R_{\mathrm{L}} = 30\ \Omega$. It can be seen from Fig. 14(a) that the dc output voltage can also be maintained as the desired value 72 V. Besides, i_{P} lags behind v_{P} and θ is $\sim$15°. This means that, with a VI and its corresponding controller, the ZVS operation has been achieved. As a result, the measured overall

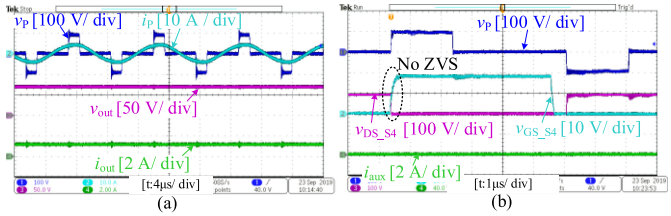

Fig. 15. Experimental waveforms of the WPT system without a VI when $R_{\mathrm{L}} = 60\ \Omega$. (a) Waveforms of v_{P}, i_{P}, v_{out}, i_{out}, and (b) waveforms of S_4.

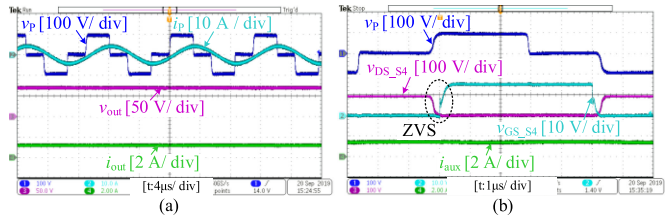

Fig. 16. Experimental waveforms of the WPT system with a VI when $R_{\mathrm{L}} = 60\ \Omega$. (a) Waveforms of v_{P}, i_{P}, v_{out}, and i_{out}. (b) Waveforms of S_4.

efficiency is $\sim$92%, which is improved by 6% compared with that of the conventional PS method.

One of the main challenges in WPT applications is the system efficiency over different loads. While previous research about WPT claims high efficiency, this attribute is usually valid only in full load condition. Wide-range ZVS is highly desired to reduce the switching loss and hence, increase the system overall efficiency. In this test, the system performances in a light-load condition ($R_{\mathrm{L}} = 90\ \Omega$) are compared by using the conventional method and the proposed method. The experimental results are provided in Figs. 15 and 16, respectively. Comparing the waveforms of the output voltage of the inverter v_{p} in Figs. 13(a) and 15(a), it is obvious that, when the system is operating in a heavy-load condition, the conducting angle α is much larger than that in a light-load condition. It can be seen from Fig. 13(b) that ZVS is not fulfilled using the conventional method. With a smaller conducting angle α, more switching loss is produced. As a result, the measured overall efficiency is decreased to $\sim$70%.

In contrast, as can be observed in Fig. 16(b), the ZVS operation can be achieved in light-load conditions with an improved $\sim$86% overall efficiency, which indicates that the WPT system using the proposed method can achieve a wide ZVS operation range.

It is obvious in Figs. 13 and 15 that without the ZVS operation, the inverter's output voltage has large ripples and oscillations, which means a large switching loss in the inverter [33], [34]. In contrast, with the ZVS operation, these voltage ripples and oscillations are mitigated, as shown in Figs. 14 and 16, which can prove that the switching loss of the inverter has been reduced [33], [34].

Besides, it can be seen from the waveforms in Figs. 13–16 that whether the operating frequency is moved away from resonant frequency, i.e., a VI is adopted at the primary side, or not, current in the primary side i_{p} can be considered as a sinusoidal

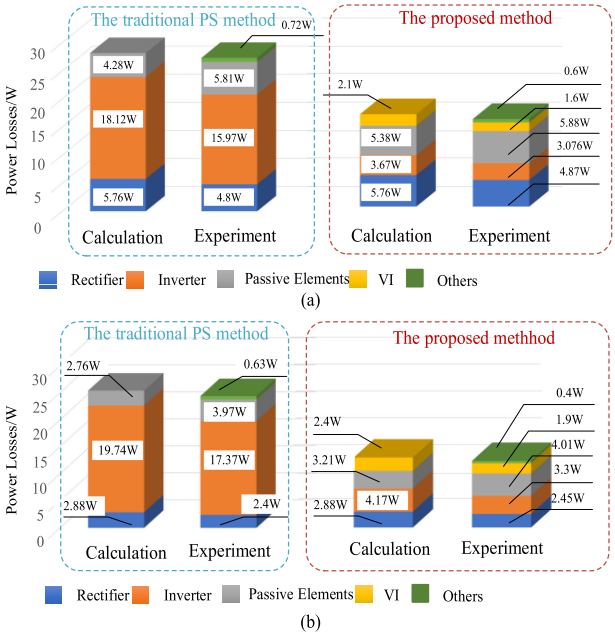

Fig. 17. Power loss comparison between the calculated results and the measured results. (a) $R_{\mathrm{L}} = 30\ \Omega$. (b) $R_{\mathrm{L}} = 60\ \Omega$.

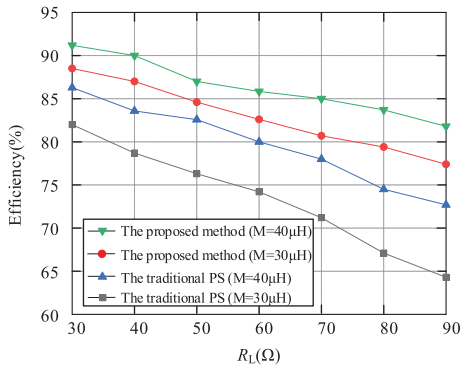

Fig. 18. Overall efficiency when $M = 30\ \mu$H and $M = 40\ \mu$H.

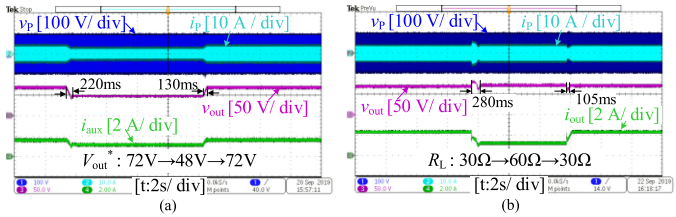

Fig. 19. Time-domain response waveforms of the WPT system with M = 40 μH. (a) Output voltage v_{out} varies from 72 to 48 V and from 48 to 72 V. (b) Load R_{L} varies from 30 to 60 Ω and from 60 to 30 Ω.

wave. Meanwhile, the waveform of v_{p} can be regarded as a step waveform. Both i_{p} and v_{p} are convenient to calculate its fundamental component for FHA. Thus, it is proved that FHA is still precise when the operating frequency is moved from the resonant frequency.

C. Losses and Overall Efficiency Analysis

To further demonstrate the power loss reduction by using the proposed VI, system power loss distributions are measured under different load resistances. As shown in Fig. 17, the power loss distributions of theoretical calculations and experiment measurements are given in detail. There are slight differences between the calculated results and the measured results due to the instrumental measurement error. It should be noted that some power losses, e.g., the contact loss on the PCB board, are relatively difficult to be measured. Therefore, the additional power loss is named as *"Others"* in Fig. 17. It is obvious that, by using the traditional PS method, i.e., without ZVS operation, the power loss in the inverter, mainly switching loss, contributes nearly half of the overall power loss. By contrast, when the WPT system realizes ZVS operation at the primary side using the proposed method, switching losses decrease considerably with effective efficiency improvement.

For a comprehensive comparison, the overall efficiencies between the PS controlled and the proposed WPT system with various M and R_{L} are given in Fig. 18. V_{dc} is 100 V and V_{out} is controlled to be constant as 72 V. With the same VI structure, the inductance of the VI can be continuously adjusted for different loads and mutual inductances. As can be seen from Fig. 18, benefitting from the wide ZVS operation range of the proposed method, the overall efficiency can be dramatically improved compared to that of the conventional PS control method under both light- and heavy-load conditions.

D. Dynamic Response

It is necessary and important to further validate the dynamic performances of the proposed method. The experimental waveform in Fig. 19(a) shows that, with $V_{\mathrm{out}}{}^*$ suddenly changed from 72 to 48 V and then increased back to 72 V, the dc output voltage V_{out} can be tightly controlled by the proposed control method with the settling times of 220 and 130 ms. The dynamic performance of the proposed control method with sudden load changes is shown in Fig. 19(b). It is seen that the proposed control method can maintain a constant output voltage (72 V) when the load resistance is changed from 30 to 60 Ω and then decreased back to 30 Ω. The settling times are only 280 and 105 ms, respectively. Both the experimental results demonstrate the fast-dynamic response of the proposed method without transient overshoots. Meanwhile, the auxiliary dc current of the VI (i_{aux}), the output voltage, and current of the inverter (v_{P} and i_{P}) are also controlled to be accurate in the steady states, which indicates that the equivalent impedance of the VI and the phase-shift angle of the inverter are exactly adjusted to achieve the ZVS operation and the constant output voltage.

VI. Conclusion

In this article, the PS control method and an auxiliary VI are proposed for the WPT system. Under magnetic coupling and load variations, a constant dc output voltage as well as a wide ZVS range can be achieved simultaneously without extra dc/dc

converters. The corresponding control diagram is provided. The proposed WPT system can operate with fixed operation frequency, which can avoid the bifurcation phenomenon. The experimental results show the effectiveness of the proposed method, and the WPT system can achieve the overall efficiency as high as 92%, which has been improved by 6% compared with that of the conventional PS method.

ACKNOWLEDGMENT

The authors would like to thank Dr. X. Li for his assistance in conducting the experiments presented in this article.

REFERENCES

[1] Y. Li, R. Mai, L. Lu, and Z. He, "Active and reactive currents decomposition based-control of angle and magnitude of current for a parallel multiinverter IPT system," *IEEE Trans. Power Electron.*, vol. 32, no. 2, pp. 1602–1614, Feb. 2017.

[2] Y. Li *et al.*, "Analysis, design, and experimental verification of a mixed high-order compensations-based WPT system with constant current outputs for driving multistring LEDs," *IEEE Trans. Ind. Electron.*, vol. 67, no. 1, pp. 203–213, Jan. 2020.

[3] J. M. Miller and A. Daga, "Elements of wireless power transfer essential to high power charging of heavy duty vehicles," *IEEE Trans. Transp. Electrific.*, vol. 1, no. 1, pp. 26–39, Jun. 2015.

[4] Y. Li, J. Hu, X. Li, and K. E. Cheng, "A flexible load-independent multi-output wireless power transfer system based on cascaded double T-resonant circuits: Analysis, design and experimental verification," *IEEE Trans. Circuits Syst. I, Reg. Papers*, vol. 66, no. 7, pp. 2803–2812, Jul. 2019.

[5] Y. Li, J. Hu, F. Chen, S. Liu, Z. Yan, and Z. He, "A new-variable-coil-structure-based IPT system with load-independent constant output current or voltage for charging electric bicycles," *IEEE Trans. Power Electron*, vol. 33, no. 10, pp. 8226–8230, Oct. 2018.

[6] Y. Li *et al.*, "Reconfigurable intermediate resonant circuit based WPT system with load-independent constant output current and voltage for charging battery," *IEEE Trans. Power Electron.*, vol. 34, no. 3, pp. 1988–1992, Mar. 2019.

[7] Y. Li *et al.*, "A new coil structure and its optimization design with constant output voltage and constant output current for electric vehicle dynamic wireless charging," *IEEE Trans. Ind. Inform.*, vol. 15, no. 9, pp. 5244–5256, Sep. 2019.

[8] S. Liu *et al.*, "Dynamic improvement of inductive power transfer systems with maximum energy efficiency tracking using model predictive control: Analysis and experimental verification," *IEEE Trans. Power Electron.*, vol. 35, no. 12, pp. 12752–12764, Dec. 2020.

[9] Y. Chen, H. Zhang, S. Park, and D. Kim, "A switching hybrid LCC-S compensation topology for constant current/voltage EV wireless charging," *IEEE Access*, vol. 7, pp. 133924–133935, 2019.

[10] K. Aditya and S. S. Williamson, "Design guidelines to avoid bifurcation in a series-series compensated inductive power transfer system," *IEEE Trans. Ind. Electron.*, vol. 66, no. 5, pp. 3973–3982, May 2019.

[11] C.-S. Wang, G. A. Covic, and O. H. Stielau, "Power transfer capability and bifurcation phenomena of loosely coupled inductive power transfer systems," *IEEE Trans. Ind. Electron.*, vol. 51, no. 1, pp. 148–157, Feb. 2004.

[12] S. Ping, A. P. Hu, S. Malpas, and D. Budgettt, "A frequency control method for regulating wireless power to implantable devices," *IEEE Trans. Biomed. Circuits Syst.*, vol. 2, no. 1, pp. 22–29, Mar. 2008.

[13] H. Li, J. Li, K. Wang, W. Chen, and X. Yang, "A maximum efficiency point tracking control scheme for wireless power transfer systems using magnetic resonant coupling," *IEEE Trans. Power Electron*, vol. 30, no. 7, pp. 3998–4008, Jul. 2015.

[14] R. Zhao, D. T. Gladwin, and D. A. Stone, "Phase shift control based maximum efficiency point tracking in resonant wireless power system and its realization," in *Proc. 42nd Annu. Conf. IEEE Ind. Electron. Soc.*, 2016, pp. 4541–4546.

[15] F. Liu, W. Lei, T. Wang, C. Nie, and Y. Wang, "A phase-shift soft-switching control strategy for dual active wireless power transfer system," in *Proc. IEEE Energy Convers. Congr. Expo.*, 2017, pp. 2573–2578.

[16] Y. Jiang, J. Liu, X. Hu, L. Wang, Y. Wang, and G. Ning, "An optimized frequency and phase shift control strategy for constant current charging and zero voltage switching operation in series-series compensated wireless power transmission," in *Proc. IEEE Energy Convers. Congr. Expo.*, 2017, pp. 961–966.

[17] D. Patil, M. Sirico, L. Gu, and B. Fahimi, "Maximum efficiency tracking in wireless power transfer for battery charger: Phase shift and frequency control," in *Proc. IEEE Energy Convers. Congr. Expo.*, Milwaukee, WI, USA, 2016, pp. 1–8.

[18] Y. Jiang, L. Wang, Y. Wang, J. Liu, M. Wu, and G. Ning, "Analysis, design, and implementation of WPT system for EV's battery charging based on optimal operation frequency range," *IEEE Trans. Power Electron.*, vol. 34, no. 7, pp. 6890–6905, Jul. 2019.

[19] Y. Fang and B. M. H. Pong, "Multiple harmonics analysis for variable frequency asymmetrical pulse width-modulated wireless power transfer systems," *IEEE Trans. Ind. Electron.*, vol. 66, no. 5, pp. 4023–4030, May 2019.

[20] J. Tian and A. P. Hu, "A DC-voltage-controlled variable capacitor for stabilizing the ZVS frequency of a resonant converter for wireless power transfer," *IEEE Trans. Power Electron.*, vol. 32, no. 3, pp. 2312–2318, Mar. 2017.

[21] Y. Jiang, J. Liu, X. Hu, L. Wang, Y. Wang, and G. Ning, "An optimized frequency and phase shift control strategy for constant current charging and zero voltage switching operation in series-series compensated wireless power transmission," in *Proc. IEEE Energy Convers. Congr. Expo.*, 2017, pp. 961–966.

[22] R. Mai, P. Yue, Y. Liu, Y. Zhang, and Z. He, "A dynamic tuning method utilizing inductor paralleled with load for inductive power transfer," *IEEE Trans. Power Electron.*, vol. 33, no. 12, pp. 10924–10934, Dec. 2018.

[23] R. A. Pinto, J. M. Alonso, M. S. Perdigao, M. F. da Silva, and R. N. do Prado, "A new technique to equalize branch currents in multiarray led lamps based on variable inductors," *IEEE Trans. Ind. Appl.*, vol. 52, no. 1, pp. 521–530, Jan./Feb. 2016.

[24] J. M. Alonso, M. A. D. Costa, M. Rico-Secades, J. Cardesin, and J. Garcia, "Investigation of a new control strategy for electronic ballasts based on variable inductor," *IEEE Trans. Ind. Electron.*, vol. 55, no. 1, pp. 3–10, Jan. 2008.

[25] D. Medini and S. Ben-Yaakov, "A current-controlled variable inductor for high frequency resonant power circuits," in *Proc. IEEE Appl. Power Electron. Conf. Expo.*, Orlando, FL, USA, 1994, pp. 219–225.

[26] B. X. Nguyen *et al.*, "An efficiency optimization scheme for bidirectional inductive power transfer systems," *IEEE Trans. Power Electron.*, vol. 30, no. 11, pp. 6310–6319, Nov. 2015.

[27] M. K. Kazimierczuk and D. Czarkowski, "Class d series-resonant inverters," in *Resonant Power Converters*, 2nd ed. Hoboken, NJ, USA: Wiley–IEEE Press, 2011.

[28] M. Zaheer, N. Patel, and A. P. Hu, "Parallel tuned contactless power pickup using saturable core reactor," in *Proc. Int. Conf. Sustain. Energy Technol.*, Dec. 2010, pp. 1–6.

[29] Z. M. Ye, P. K. Jain, and P. C. Sen, "Full-bridge resonant inverter with modified PSM for HFAC power distribution systems," *IEEE Trans. Ind. Electron.*, vol. 54, no. 5, pp. 2831–2845, Oct. 2007.

[30] Z. Liu and H. Lee, "A 100V gate driver with sub-nanosecond-delay capacitive-coupled level shifting and dynamic timing control for ZVS-based synchronous power converters," in *Proc. IEEE Custom Integr. Circuits Conf.*, 2013, pp. 1–4.

[31] I. Castro *et al.*, "Analytical switching loss model for super junction MOSFET with capacitive nonlinearities and displacement currents for dc–dc power converters," *IEEE Trans. Power Electron.*, vol. 31, no. 3, pp. 2485–2495, Mar. 2016.

[32] Y. Jiang, L. Wang, Y. Wang, J. Liu, X. Li, and G. Ning, "Analysis, design and implementation of accurate ZVS angle control for EV's battery charging in wireless high power transfer," *IEEE Trans. Ind. Electron.*, vol. 66, no. 5, pp. 4075–4085, May 2019.

[33] E. Rozanov and S. Ben-Yaakov, "Analysis of current-controlled inductors by new spice behavioral model," *HAIT J. Sci. Eng. B*, vol. 2, no. 3/4, pp. 558–570, 2005.

[34] C. Leonardi, A. Raciti, F. Frisina, R. Letor, and S. Musumeci, "A new power MOSFET model including the variation of parameters with the temperature," in *Proc. 2nd IEEE Int. Caracas Conf. Devices, Circuits Syst.*, 1998, pp. 261–266.

[35] H. Hu, T. Cai, S. Duan, X. Zhang, J. Niu, and H. Chen, "An optimal variable frequency phase shift control strategy for ZVS operation within wide power range in IPT systems," *IEEE Trans. Power Electron.*, vol. 35, no. 5, pp. 5517–5529, May 2020.

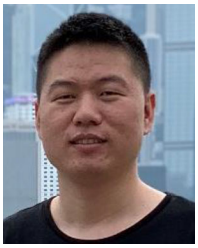

Yong Li (Member, IEEE) received the B.Sc. and Ph.D. degrees from the School of Electrical Engineering, Southwest Jiaotong University, Chengdu, China, in 2013 and 2017, respectively.

From 2017 to 2018, he was a Research Associate with the Department of Electrical Engineering, The Hong Kong Polytechnic University, Hong Kong, where he became a Postdoctoral Fellow. He is currently an Associate Professor with Southwest Jiaotong University. His main research interests include wireless power transfer and microgrids.

Dr. Li is a Guest Editor for *Electronics* for a special issue "Wireless Power Transfer and Its Applications."

Shunpan Liu received the B.S. degree in electrical engineering and automation in 2018 from the School of Electrical Engineering, Southwest Jiaotong University, Chengdu, China, where he is currently working toward the Ph.D. degree.

His main research interests include wireless power transfer, especially on control method and circuit topology of dynamic inductive power transfer systems.

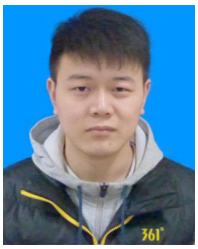

Xiao Zhu is currently working toward the master's degree in electrical engineering and automation with the School of Electrical Engineering, Southwest Jiaotong University, Chengdu, China.

His main research interests include wireless power transfer.

Jiefeng Hu (Senior Member, IEEE) received the Ph.D. degree in electrical engineering from the University of Technology Sydney (UTS), Sydney, NSW, Australia, in 2013.

He was involved in the research of minigrids in Commonwealth Scientific and Industrial Research Organization (CSIRO), Newcastle, NSW, Australia. He was an Assistant Professor with Hong Kong Polytechnic University, Hong Kong. He is currently an Associate Professor with Federation University Australia, Ballarat, VIC, Australia. His research interests include power electronics, renewable energy, and smart microgrids.

Dr. Hu is an Editor for the IEEE TRANSACTIONS ON ENERGY CONVERSION and a Guest Editor for the IEEE TRANSACTIONS ON INDUSTRIAL ELECTRONICS for a special issue "Applications of Predictive Control in Microgrids."

Min Zhang received the master's degree in electrical engineering and automation in 2012 from the School of Electrical Engineering, Southwest Jiaotong University, Chengdu, China, where he is currently working toward the Ph.D. degree.

His main research interests include wireless power transfer.

Ruikun Mai (Member, IEEE) received the B.Sc. and Ph.D. degrees from the School of Electrical Engineering, Southwest Jiaotong University, Chengdu, China, 2004 and 2010, respectively.

He is currently a Professor with the School of Electrical Engineering, Southwest Jiaotong University. His research interests include wireless power transfer and its application in railway systems, power system stability, and control.

Zhengyou He (Senior Member, IEEE) received the B.Sc. and M.Sc. degrees in computational mechanics from Chongqing University, Chongqing, China, in 1992 and 1995, respectively, and the Ph.D. degree from the School of Electrical Engineering, Southwest Jiaotong University, Chengdu, China, in 2001.

He is currently a Professor with the School of Electrical Engineering, Southwest Jiaotong University. His research interests include signal processing and information theory applied to electrical power systems, and application of wavelet transforms in power systems.